Flexoelectricity and the Formation of Carbon Nanoparticles in Flames

Jacob W. Martin,[†,‡] Maria Botero,[¶,‡] Radomir I. Slavchov,[†] Kimberly Bowal,[†] Jethro Akroyd,[†] Sebastian Mosbach,[†] and Markus Kraft[*,†,§,‡,‖]

[†]*Department of Chemical Engineering and Biotechnology, University of Cambridge, Cambridge CB3 0AS, UK*

[‡]*Cambridge Centre for Advanced Research and Education in Singapore (CARES), Singapore 138602*

[¶]*Department of Mechanical Engineering, National University of Singapore, Singapore 117576*

[§]*School of Chemical and Biomedical Engineering, Nanyang Technological University, Singapore 637459*

[‖]*Current address: West Site, Philippa Fawcett Drive, Cambridge CB3 0AS, UK*

E-mail: mk306@cam.ac.uk

Phone: +44 (0)1223 762784

ABSTRACT

The formation of carbon nanoparticles in flames involves a nucleation step that remains poorly understood. Experimentally, carbon nuclei formation is known to depend strongly on the electrical aspects of combustion but modes of interaction between charged species in the flame and carbon precursors have yet to be found. We present evidence for flexoelectrically polarised aromatics contributing to carbon nanoparticulate nucleation. We imaged the nascent nanoparticles using high resolution transmission electron microscopy, which revealed that the majority of aromatics in the early carbon nanoparticles are fullerene-like and curved. The curvature induces a significant molecular flexoelectric dipole moment in the polyaromatic hydrocarbons. This electric polarization allows these molecules to strongly interact with chemi-ions produced during combustion, which we demonstrate using electronic structure calculations. The results indicate that the physical interaction between fullerene-like polar aromatics and chemi-ions is critically assisting the nucleation, and opens a new route to reduce pollution and improve flame-produced nanomaterials.

INTRODUCTION

Air pollution from combustion leads to respiratory diseases[1] and contributes to the warming of the planet.[2] Flames can also synthesize a variety of useful carbon particles and nanomaterials for applications in lithium ion batteries, conductive inks, and solar cells.[3] The critical step in reducing harmful particulates or controlling the synthesis of useful carbon nanoparticles in flames is the nucleation process where pericondensed polycyclic aromatic molecules (PAHs) form carbon nuclei 1–3 nm in diameter. Yet despite many decades of research on carbon formation during combustion, the mechanism of this nucleation process remains elusive.[4]

The electrical aspects of carbon nanoparticle nucleation in flames, such as charging processes and the influence of external electric fields, have been studied since the 1950s.[5,6]

Chemical reactions with vibrationally excited carbyne (CH*) readily produce chemi-ions, such as the formyl (CHO^+), cyclopropenyl ($C_3H_3^+$) and hydronium (H_3O^+) cations, at significant concentrations in the flame ($10^{15} - 10^{17}$ m^{-3}).[5,6] As these ions are consumed in the combustion process, the carbon nuclei form in similar concentrations ($10^{14} - 10^{16}$ m^{-3} [7–9]). Recently, high resolution particle analyzers revealed that up to 95% of the sub-3 nm carbon nuclei are charged.[10] A proportion of these nuclei grow into what are referred to as primary particles (20–30 nm in diameter), eventually coagulating into large, multiply charged fractal aggregates.[11]

The many charged molecules and particles in flames can be manipulated using electric fields[12,13] and a resulting significant reduction or complete eradication of particulates has been demonstrated.[13,14] Figure 1 shows the impact of an electric field on the flame in a counterflow diffusion ethylene burner. The disappearance of the luminous yellow carbon particulates is clearly visible and has been ascribed to removal of the charged nuclei from the pyrolysis zone by the field.[6] Recent laser induced incandescence and fluorescence imaging of the carbon particulates and molecular species, respectively, in a similar burner configuration, confirmed that the electric field removed the carbon particulates whilst the gas phase chemistry was only minimally changed, suggesting the field primarily influenced the process of nucleation.[13]

The concentration of ions in a flame can be artificially increased through the addition of alkali and other metals, which easily ionize at flame temperatures. Electron microscopy[15] and small angle X-ray diffraction[16] revealed that primary particles increased in number and decreased in size with these metal additives, with significant reductions in the mass of particulates produced (50–90% reduction being reported for polystyrene combustion[17]). The role of metal ions in carbon particulate reduction was considered to be due to the ions stabilizing nuclei, producing large numbers of smaller carbon particles with increased surface area allowing for their rapid oxidation and destruction.[18] A similar effect was achieved by application of a strong electric field to the flame, drawing positive chemi-ions from the flame

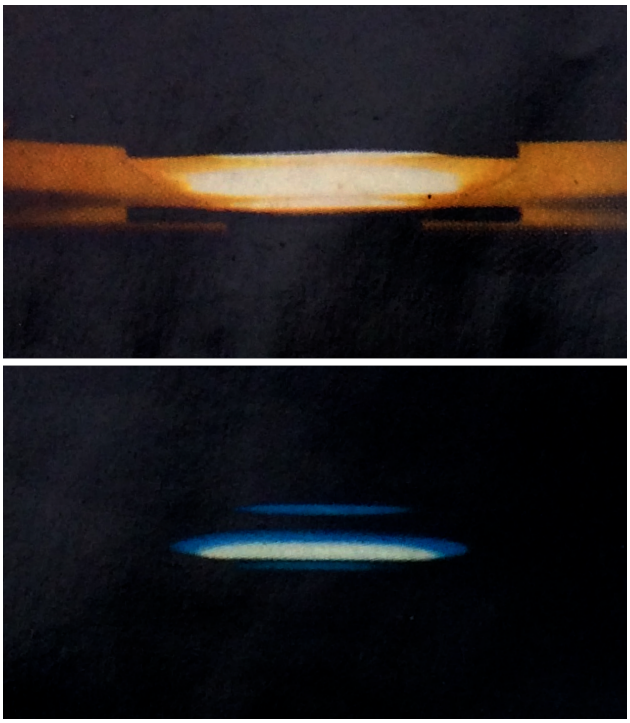

Figure 1: Counterflow $C_2H_4/O_2/N_2$ diffusion flame without (top) and with (bottom) an electric potential difference of 1 kV applied. Luminous carbon particulates (yellow) disappear from the flame by application of the field (from Lawton and Weinberg[6] *'Electrical aspects of combustion'*, used with permission from Oxford University Press).

zone to the pyrolysis zone.[19] This effect has found application in the design of organometallic anti-smoke additives for diesel engines.[20] The ability of various metal ions to decrease smoke was found to follow the series Ba > Ca > Ni > Na, K, Zn. According to Magaril and Magaril, Ba and Ca have stronger effects due to their low ionization energies; the series suggests that the ratio (ionic charge)^2/(ionic radius) is also a factor, which is evidence for nucleation on ions.[21]

While the suggestion of ions assisting nucleation is not new, the search for the interaction between ions and the aromatic precursors responsible for the observed effects has been unsuccessful. One suggestion was that the effect is chemical kinetic in nature:[8,19] Calcote assumed that chemi-ions may promote rapid polymerization due to ion-induced dipole inter-

actions, forming polycyclic aromatic hydrocarbons (PAHs) and then larger nuclei. However, this mechanism cannot explain the effect of Ba^{2+} and Ca^{2+}. The chemical mechanism for PAH formation was instead found to be due to the radical mechanism (hydrogen abstraction and acetylene addition, HACA); the rate of ion-enhanced polymerization reactions was found to be too low at flame temperatures.[4,22] The possibility of heterogeneous nucleation of planar PAHs on ions has also been investigated using electronic structure calculations.[23] The electrostatic interaction between a chemi-ion and planar PAHs was found to result in binding of the ion around the rim of the planar PAH; however, energies were insufficient to stabilize the ion-PAH complexes at temperatures at which carbon nanoparticles form in the flame (1300–1500 K).[24]

What interaction is then holding the PAH molecules and the charge together in a nucleus? Recent electron microscopy of carbon particulates has demonstrated that they contain a significant number of non-planar PAH molecules.[25,26] Furthermore, curved aromatics such as corannulene have been extracted from carbon particulates,[27,28] and even completely closed carbon cages (e.g., C_{60} and C_{70} fullerenes) have been synthesized in low-pressure benzene flames.[29,30] PAHs can curve through the integration of non-hexagonal rings into their structure that become completely surrounded by hexagonal rings. The process has been predicted to occur through the HACA mechanism of acetylene addition to an armchair functional site possessing a pentagonal ring:[31]

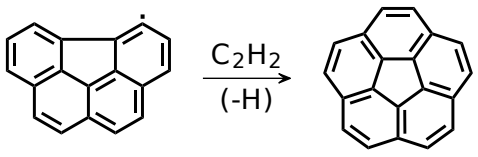

This mechanism suggests that the precursors of the curved molecules are smaller PAHs containing five-membered rings, which are well-known to be among the most abundant PAHs in the flame (as much as 25% of those smaller than C_{24}[5]). Despite curved PAHs being less energetically favored compared with planar PAH, kinetic analysis suggested that the pentagonal ring enclosure does occur at flame conditions, albeit at a slower rate compared

to hexagonal ring integration.[32,33]

Something peculiar about curved PAHs is that they are highly polar molecules. We recently performed electronic structure calculations on large curved aromatic molecules[34] and found a significant flexoelectric dipole moment for curved PAHs (4–6.5 D – approximately two to three times that of water at 1.85 D[35]). Many small flat PAHs containing pentagons are also polar.[36] In addition, the dispersion and ion-induced dipole interactions between an ion and a curved PAH are significantly higher for an ion attached at the concave side of the curved PAH compared to ion-planar PAHs (due to closer contact). Thus, the interaction between polar PAHs and ions is stronger and much more long-ranged than the planar PAH-ion, which has applications including the use of curved PAHs to store large amounts of lithium in battery anodes.[37]

In this work, we present evidence of large amounts of polar aromatics in the nascent carbon nanoparticles and calculate significant binding energies between a representative polar PAH with the cation $C_3H_3^+$.

METHODS

Carbon particulates were sampled thermophoretically from an ethylene coflow diffusion flame using a rapid solenoid injector and imaged with an electron microscope (Figure 2a and b), where fringes (elongated dark regions where the electron beam intensity was reduced) in the high resolution transmission electron microscopy (HRTEM) micrograph correspond to imaging across the plane of an aromatic molecule (see Figure 2c and d).

We analyzed these fringes using custom image-analysis software which skeletonizes the fringes into discrete lines for which geometrical parameters were calculated: length (L), end-to-end distance (C), and tortuosity ($\tau = L/C$). We have previously benchmarked the accuracy of the fringe analysis against simulated HRTEM images of planar PAHs.[25] Our software was modified to analyze the fringes of 209 primary particles, as a function of the

radius from the center of the particle and the sampling height above the burner. The earliest carbon nanoparticulates that could be sampled were at 10 mm above the burner. These early particles, ∼10 nm in diameter, provide insight into the aromatic content in the carbon nuclei, which cannot be directly sampled thermophoretically or imaged due to their small size. Figure 2c and d shows the skeletonized fringes from two representative primary particles – one early particle 10 mm above the burner, where luminosity has yet to develop, and another from the tip (at 49 mm above the burner) – along with the electron micrographs of the particles before image processing. For the radial dependence, fringes were partitioned into five equal-radius concentric spherical shells, and the fringe size and tortuosity distributions were calculated for each shell. The distributions were positively skewed towards longer fringes; therefore, we preferred to use the median length and tortuosity instead of the mean.

RESULTS AND DISCUSSION

The size of the molecular fragments in the nanoparticles can be inferred from the fringe length. Figure 2f shows the fringe lengths across all heights above the burner. The fringes' median size ranges from 0.9–1.2 nm, corresponding to aromatics with 14–22 aromatic rings (assuming a circular pericondensed aromatic[25]). The results for the lowest height above the burner (10 mm) provide insight into the species present at nuclei formation; there, $L = 0.9 - 1.05$ nm, corresponding to a size of 15 aromatic rings, consistent with optical band gap measurements[25] and mass spectrometry.[38]

The amount of curved PAHs in the carbon nanoparticles was quantified by analyzing the tortuosity of the fringes. The tortuosity is a measure of the curvature, and therefore, of the polarity of the molecular fragments corresponding to a fringe. The majority of fringes in the nanoparticles at 10 mm above the burner contained a single peak in the curvature and no inflection, indicating the incorporation of pentagons, not heptagons, into the aromatic

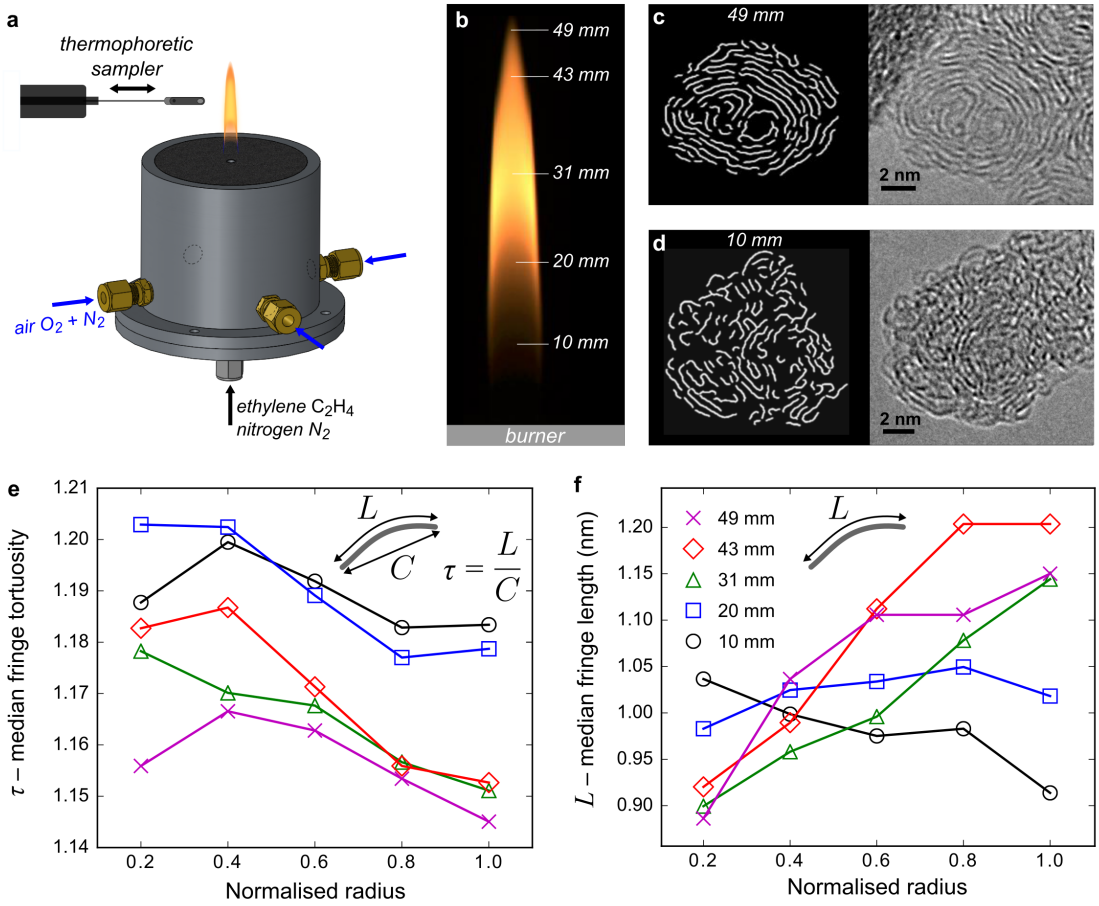

Figure 2: **a**, Schematic of the co-flow diffusion flame used and the rapid solenoid injector, and **b**, sampling positions. **c-d**, Skeletonized and unprocessed HRTEM images of primary carbon nanoparticulates for 10 and 49 mm heights above the burner (particles are not shown to scale but have radii of 9.5–10 and 8.5–10.2 nm; unprocessed images are also shown). **e-f**, Fringe median length and tortuosity as a function of the radial distance normalized to the size of the primary particles for various heights above the burner (standard errors ±0.01 for τ, and ±0.03 nm for L).

molecules at this low height (which was also observed by Wang et al. [26]). As seen in Figure 2e, the fringes became less tortuous as the carbon particulates progress through the flame, initially starting at τ =1.18–1.20 and finally leaving the flame with values of τ =1.15–1.17.

The correspondence between the tortuosity and number of pentagons was analyzed by simulating HRTEM images of curved PAHs with the similar number of aromatic rings (15) as seen in the early flame, with three, two, and one enclosed pentagons (Figure 3a, b and c). The same fringe analysis software was applied to these simulated images and tortuosity values of 1.37, 1.20, and 1.13 were found. Small crosslinked PAHs were also analyzed as alternative species that could produce tortuous fringes (see supplementary Figure S3). The orientation with the maximum fringe tortuosity we could produce for a non-pentagonal PAH crosslinked species was τ =1.15, a value similar to τ of a curved PAH with a single pentagonal ring. We therefore considered fringes with tortuosity values >1.15 to be predominantly due to pentagon integration and not crosslinked species. This cutoff underestimates the amount of curved aromatics due to pentagon integration as it is not possible to distinguish them from crosslinked PAHs. Using this cutoff we calculated that for the lowest sampled height, at least 62.5% of the fringes indicated pentagon integration. This amount of pentagon integration is higher than the values 28–49% found previously for mature carbon particulates.[26,33] These lower values can be explained by the age of the particles; indeed, the fringe analysis for carbon particulates sampled from the late stages of the flame have considerably flatter and longer fringes, indicating a carbonization process leading to removal of embedded pentagonal rings.

The polarity of curved PAHs in the carbon particulates at 10 mm above the burner can be estimated based on the median fringe length (L ~1 nm) and tortuosity (τ ~1.2) suggested from HRTEM image analysis of early carbon nanoparticles, which correspond to the curved PAH containing two pentagons (Figure 3b). We calculated a dipole moment of 5.32 D for this species using the methodology developed previously.[34] Figure 3d shows the electrostatic potential perpendicular to the aromatic plane of the PAH and reveals significant charge polarization due to the flexoelectric effect. The electrostatic potential indicates strong binding sites for cations on the convex and concave surfaces of the aromatic plane.

For chemi-ions and curved PAHs to interact at flame temperatures where carbon par-

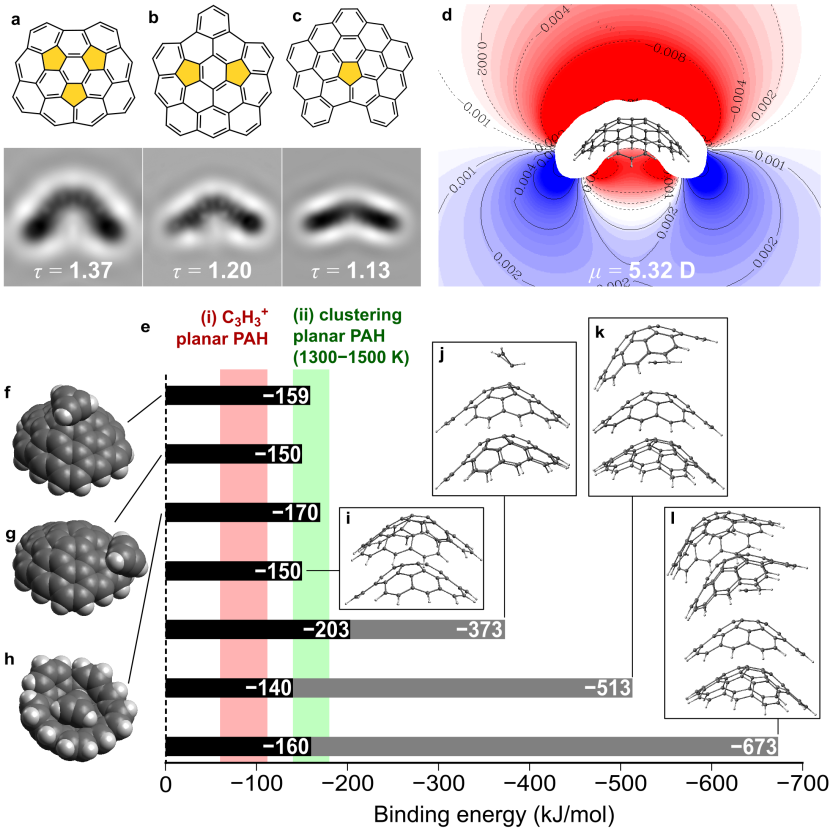

Figure 3: **a-c,** Curved aromatics with three, two, and one pentagons, respectively, with simulated HRTEM images (with their corresponding calculated tortuosity value). **d,** Electrostatic potential perpendicular to the aromatic plane for the curved PAH with two pentagons (isovalues of the potential are shown in a.u.). **e**, Dissociation energies for the cation-curved PAH complexes (black bar). The red region (i) shows the range of binding energies calculated previously for planar PAHs binding to $C_3H_3^+$;[23] the green (ii) shows the region of binding energies that were found to allow large planar PAHs to cluster at 1300–1500 K.[39] **f-h,** Optimized geometries of binding sites for the chemi-ion $C_3H_3^+$ on the curved PAH **b**. **i,** Geometries of the dimer of the curved PAH **b**. **h-j,** Cluster geometries for the dimer, trimer and tetramer with the chemi-ion $C_3H_3^+$ (grey bars show complexes' total binding energies).

ticulates form (1300-1500 K), large intermolecular interaction energies are required to stabilize molecular clusters. For planar PAHs with 13–19 rings we have previously determined the dissociation energy required to stabilize clusters at these temperatures at $E_d = -140$–180 kJ/mol (shown as the green range (i) in Figure 3e).[39] The chemi-ion $C_3H_3^+$ is the most abundant cation in sooting flames and is a likely candidate for a nucleation center in a nucleation mechanism.[9] Chen and Wang recently used coupled cluster calculations to analyze the binding of $C_3H_3^+$ with planar PAHs.[23] They found that the stable configurations occurred when the cation bonded around the rim of the planar PAH, saturating for PAHs containing more than five aromatic rings at binding energies of −60–112 kJ/mol (shown as the grey range (ii) in Figure 3e), which is insufficient to stabilize these complexes under flame-relevant temperatures.

We calculated the binding energies between the curved PAH we identified as a likely component in carbon particulates (Figure 3b) and $C_3H_3^+$ using hybrid density functional theory with a dispersion correction.[40,41] This level of theory has previously been found to accurately predict binding energies of cation-benzene complexes and of dimers of the curved PAH corannulene (within ±4 kJ/mol) compared to benchmark coupled cluster calculations.[42,43] We confirmed that this methodology also correctly reproduces the dipole moment of corannulene compared with our previous calculations,[34] indicating that the electrostatic and dispersion interactions are each being described with satisfactory accuracy. Figure 3f-h shows the geometries of the three most stable binding sites of $C_3H_3^+$. A similar binding site to planar PAHs was found around the rim of the curved PAH (Figure 3g), however, unlike the planar geometries, binding on the center of the aromatic faces was stronger than on the rim. The binding site with the highest binding energy was found for the concave surface (Figure 3h), where the cupped geometry enhanced the dispersion interactions and the negative electric potential due to the π-orbitals. The binding site at the center of the convex surface (Figure 3f) is dominated by the flexoelectric dipole-ion interaction: a classical electrostatic charge-dipole interaction at the intermolecular distance of 3 Å gives a similar binding energy

of −171 kJ/mol using the dipole moment 5.32 D calculated earlier. Figure 3i shows the curved PAH homodimer with an energy of $E_{\mathrm{d}} = -150$ kJ/mol, which is comparable to a similar sized planar PAH of −144 kJ/mol (interpolated from the Totton et al. benchmark calculations based on the number of carbon atoms[39]) indicating similar clustering behavior to planar PAHs is expected for homogeneous nucleation of this curved PAH.

For larger clusters of the curved PAH stabilized by an ion, geometry optimizations were performed from different possible starting geometries to ensure stable energy minima were found for the dimer, trimer, and tetramer (with the binding energies E_{b} shown in Figure 3j-l as grey bars). Unlike planar PAHs, which see a significant decrease in binding energy with a chemi-ion for subsequent additions after the dimer, the binding energies of clusters of curved PAHs stabilized with a chemi-ion continues to increase linearly towards that of the tetramer.[23] The stacking geometry of the curved PAH is stabilized by the dispersion and dipole-dipole interactions being further strengthened by the electrostatic and inductive interactions with the chemi-ion. We also calculated the dissociation energies E_{d} as the energy required to remove a monomer from the complex (shown in Figure 3j-l as black bars). All of the dissociation energies calculated between the chemi-ion $C_3H_3^+$ with a representative polar curved PAH are found to be in the range to allow planar PAH to cluster at flame temperatures suggesting these interactions play a role in stabilizing carbon particulate nuclei.

In order to fully understand the role of chemi-ions in nuclei formation further work is needed. Firstly, more experimental work is required to determine the amounts of polar and non-polar aromatic PAHs present in the gas phase where nucleation is taking place. Secondly, computational work is required to determine whether these collections of curved PAHs form nuclei around chemi-ions at flame temperatures and how this mechanism competes with homogeneous nucleation or a chemical inception mechanism under different combustion conditions. However, we can consider some potential applications of such an ionic mechanism. It could provide a new route to reduce carbon particulate pollution. Additives could be incorporated into fuels or engine operating conditions modified to reduce the curvature integrated

into aromatics in flames in order to reduce interaction energies with cations and thereby reduce production of particulates. This understanding could also improve flame synthesis of nanoparticles such as fullerenes or graphene by inhibiting the pathways to particulate formation.

CONCLUSIONS

To conclude, we present strong evidence of enrichment of the nascent carbon nanoparticles in curved polar PAH molecules. If 25% of the PAHs found in the gas phase contain pentagonal rings[5] and that in the earliest carbon nanoparticles we could sample the content of curved molecular fragments is at least 62.5%, as it follows from the fringe analysis of the HRTEM images, then curved species appear to be enriched in early carbon nanoparticles. The result can be explained with nucleation of curved PAHs on ions in the flame; the likelihood of this hypothesis is demonstrated by the high binding energies of the flame ion $C_3H_3^+$ to a representative curved PAH, and with the high stability of larger complexes of several curved polar PAHs and the ion, as computed from electronic structure calculations. While further details and applications remain to be explored, this work provides for the first time evidence of the significant role of the curved PAHs and the polar PAH-ion interaction in carbon particulate formation in flames.

ACKNOWLEDGEMENT

This project is supported by the National Research Foundation (NRF), Prime Minister's Office, Singapore under its Campus for Research Excellence and Technological Enterprise (CREATE) programme. This work used the ARCHER UK National Supercomputing Service (http://www.archer.ac.uk).

SUPPORTING INFORMATION DESCRIPTION

Experimental procedures and simulations details can be found in the supplementary information.

REFERENCES

(1) Landrigan, P. J.; Fuller, R.; Acosta, N. J. R.; Adeyi, O.; Arnold, R.; Basu, N. N.; Baldé, A. B.; Bertollini, R.; Bose-O'Reilly, S.; Boufford, J. I. et al. ; The lancet commission on pollution and health. *Lancet* **2017**,

(2) McConnell, J. R.; Edwards, R.; Kok, G. L.; Flanner, M. G.; Zender, C. S.; Saltzman, E. S.; Banta, J. R.; Pasteris, D. R.; Carter, M. M.; Kahl, J. D. W. 20th-century industrial black carbon emissions altered arctic climate forcing. *Science* **2007**, *317*, 1381–1384.

(3) Rong, Y.; Hou, X.; Hu, Y.; Mei, A.; Liu, L.; Wang, P.; Han, H. Synergy of ammonium chloride and moisture on perovskite crystallization for efficient printable mesoscopic solar cells. *Nat. Commun.* **2017**, *8*, 14555.

(4) Wang, H. Formation of nascent soot and other condensed-phase materials in flames. *Proc. Combust. Inst.* **2011**, *33*, 41–67.

(5) Fialkov, A. Investigations on ions in flames. *Prog. Energy Combust. Sci.* **1997**, *23*, 399–528.

(6) Lawton, J.; Weinberg, F. *Electrical aspects of combustion*; Clarendon P., 1969.

(7) Haynes, B. S.; Wagner, H. G. Soot formation. *Prog. Energy Combust. Sci.* **1981**, *7*, 229–273.

(8) Calcote, H. F.; Olson, D. B.; Keil, D. G. Are ions important in soot formation? *Energy Fuels* **1988**, *2*, 494–504.

(9) Hayhurst, A. N.; Jones, H. R. N. Ions and soot in flames. *J. Chem. Soc., Faraday Trans. 2* **1987**, *83*, 1.

(10) Wang, Y.; Kangasluoma, J.; Attoui, M.; Fang, J.; Junninen, H.; Kulmala, M.; Petäjä, T.; Biswas, P. The high charge fraction of flame-generated particles in the size range below 3 nm measured by enhanced particle detectors. *Combust. Flame* **2017**, *176*, 72–80.

(11) Onischuk, A. A.; Di Stasio, S.; Karasev, V. V.; Baklanov, A. M.; Makhov, G. A.; Vlasenko, A. L.; Sadykova, A. R.; Shipovalov, A. V.; Panfilov, V. N. Evolution of structure and charge of soot aggregates during and after formation in a propane/air diffusion flame. *J. Aerosol Sci.* **2003**, *34*, 383–403.

(12) Saito, M.; Arai, T.; Arai, M. Control of soot emitted from acetylene diffusion flames by applying an electric field. *Combust. Flame* **1999**, *119*, 356–366.

(13) Park, D. G.; Choi, B. C.; Cha, M. S.; Chung, S. H. Soot reduction under DC electric fields in counterflow non-premixed laminar ethylene flames. *Combust. Sci. Technol.* **2014**, *186*, 644–656.

(14) Mayo, P. J.; Weinberg, F. J. On the size, charge and number-rate of formation of carbon particles in flames subjected to electric fields. *Proc. R. Soc. A* **1970**, *319*, 351–371.

(15) Simonsson, J.; Olofsson, N. E.; Bladh, H.; Sanati, M.; Bengtsson, P. E. Influence of potassium and iron chloride on the early stages of soot formation studied using imaging LII/ELS and TEM techniques. *Proc. Combust. Inst.* **2017**, *36*, 853–860.

(16) Di Stasio, S.; Legarrec, J. L.; Mitchell, J. B. Synchrotron radiation studies of additives in combustion, II: Soot agglomerate microstructure change by alkali and alkaline-earth metal addition to a partially premixed flame. *Energy Fuels* **2011**, *25*, 916–925.

(17) Chung, S. L.; Lai, N. L. Suppression of soot by metal additives during the combustion of polystyrene. *J. Air Waste Manage. Assoc.* **1992**, *42*, 1082–1088.

(18) Howard, J. B.; Kausch, W. J. Soot control by fuel additives. *Prog. Energy Combust. Sci.* **1980**, *6*, 263–276.

(19) Place, E. R.; Weinberg, F. J. Electrical control of flame carbon. *Proc. R. Soc. A* **1966**, *289*, 192–205.

(20) Magaril, E. R.; Magaril, R. Z. *Engine fuels*; KDU: Moscow, 2008; p 134.

(21) Kashchiev, D. *Nucleation*; Butterworth-Heinemann, 2000.

(22) Frenklach, M.; Ramachandra, M.; Matula, R. Soot formation in shock-tube oxidation of hydrocarbons. *Symp. (Int.) Combust.* **1985**, *20*, 871 – 878.

(23) Chen, D.; Wang, H. Cation-π interactions between flame chemi-ions and aromatic compounds. *Energy Fuels* **2017**, *31*, 2345–2352.

(24) Glassman, I. Soot formation in combustion processes. *Symp. (Int.) Combust.* **1989**, *22*, 295–311.

(25) Botero, M. L.; Adkins, E. M.; González-Calera, S.; Miller, H.; Kraft, M. PAH structure analysis of soot in a non-premixed flame using high-resolution transmission electron microscopy and optical band gap analysis. *Combust. Flame* **2016**, *164*, 250–258.

(26) Wang, C.; Huddle, T.; Huang, C. H.; Zhu, W.; Vander Wal, R. L.; Lester, E. H.; Mathews, J. P. Improved quantification of curvature in high-resolution transmission electron microscopy lattice fringe micrographs of soots. *Carbon* **2017**, *117*, 174–181.

(27) Lafleur, A. L.; Howard, J. B.; Marr, J. A.; Yadav, T. Proposed fullerene precursor corannulene identified in flames both in the presence and absence of fullerene production. *J. Phys. Chem.* **1993**, *97*, 13539–13543.

(28) Wu, X. Z.; Yao, Y. R.; Chen, M. M.; Tian, H. R.; Xiao, J.; Xu, Y. Y.; Lin, M. S.; Abella, L.; Tian, C. B.; Gao, C.-L. et al. ; Formation of curvature subunit of carbon in combustion. *J. Am. Chem. Soc.* **2016**, *138*, 9629–9633.

(29) Gerhardt, P.; Lffler, S.; Homann, K. Polyhedral carbon ions in hydrocarbon flames. *Chem. Phys. Lett.* **1987**, *137*, 306 – 310.

(30) Richter, H.; Labrocca, A. J.; Grieco, W. J.; Taghizadeh, K.; Lafleur, A. L.; Howard, J. B. Generation of higher fullerenes in flames. *J. Phys. Chem. B* **1997**, *101*, 1556–1560.

(31) Frenklach, M.; Ebert, L. B. Comment on the proposed role of spheroidal carbon clusters in soot formation. *J. Phys. Chem.* **1988**, *92*, 561–563.

(32) Whitesides, R.; Frenklach, M. Detailed kinetic Monte Carlo simulations of graphene-edge growth. *J. Phys. Chem.. A* **2010**, *114*, 689–703.

(33) Yapp, E. K.; Wells, C. G.; Akroyd, J.; Mosbach, S.; Xu, R.; Kraft, M. Modelling PAH curvature in laminar premixed flames using a detailed population balance model. *Combust. Flame* **2017**, *176*, 172–180.

(34) Martin, J. W.; Slavchov, R. I.; Yapp, E. K. Y.; Akroyd, J.; Mosbach, S.; Kraft, M. The polarization of polycyclic aromatic hydrocarbons curved by pentagon incorporation: the role of the flexoelectric dipole. *J. Phys. Chem. C* **2017**, *121*, 27154–27163.

(35) Shostak, S. L.; Ebenstein, W. L.; Muenter, J. S. The dipole moment of water. I. Dipole moments and hyperfine properties of H_2O and HDO in the ground and excited vibrational states. *J. Chem. Phys.* **1991**, *94*, 5875.

(36) Martin, J. W.; Bowal, K. L.; Menon, A.; Slavchov, R. I.; Akroyd, J.; Mosbach, S.; Kraft, M. Polar curved polycyclic aromatic hydrocarbons in soot formation. *Proc. Combust. Inst.* **2018**, *Available online 19 June 2018*.

(37) Zabula, A. V.; Filatov, A. S.; Spisak, S. N.; Rogachev, A. Y.; Petrukhina, M. A. A main group metal sandwich: five lithium cations jammed between two corannulene tetraanion decks. *Science* **2011**, *333*, 1008–1011.

(38) Lighty, J.; Romano, V.; Sarofim, A.; Bockhorn, H.; D'Anna, A.; Sarofim, A.; Wang, H. *Combustion generated fine carbonaceous particles*; KIT Scientific Publishing, 2009.

(39) Totton, T. S.; Misquitta, A. J.; Kraft, M. A quantitative study of the clustering of polycyclic aromatic hydrocarbons at high temperatures. *Phys. Chem. Chem. Phys.* **2012**, *14*, 4081–94.

(40) Grimme, S. Semiempirical GGA-type density functional constructed with a long-range dispersion correction. *J. Comput. Chem.* **2006**, *27*, 1787–1799.

(41) Frisch, M. J.; Trucks, G. W.; Schlegel, H. B.; Scuseria, G. E.; Robb, M. A.; Cheeseman, J. R.; Scalmani, G.; Barone, V.; Petersson, G. A.; Nakatsuji, H. et al. ; Gaussian 09, Revision A 02. 2009.

(42) Janowski, T.; Pulay, P.; Sasith Karunarathna, A. A.; Sygula, A.; Saebø, S. Convex-concave stacking of curved conjugated networks: Benchmark calculations on the corannulene dimer. *Chem. Phys. Lett.* **2011**, *512*, 155–160.

(43) Neves, A. R.; Fernandes, P. A.; Ramos, M. J. The accuracy of density functional theory in the description of cation-π and π-hydrogen bond interactions. *J. Chem. Theory Comput.* **2011**, *7*, 2059–2067.

TOC IMAGE

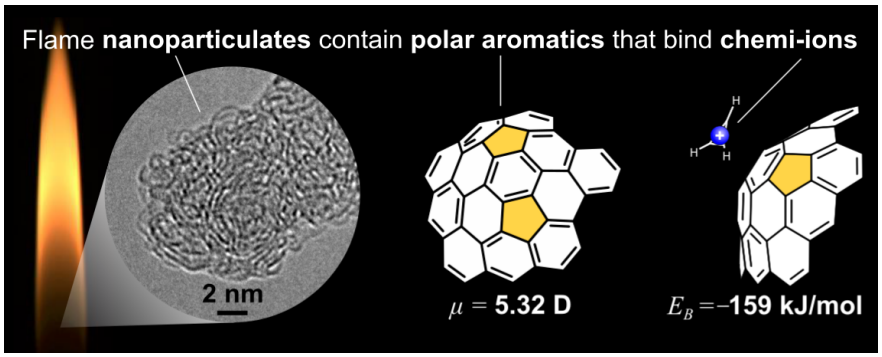
Flame **nanoparticulates** contain **polar aromatics** that bind **chemi-ions**
2 nm
μ = 5.32 D
E_B = –159 kJ/mol